Two-Dimensional Wess-Zumino Models at Intermediate Couplings

Tobias Kästner, Georg Bergner, Sebastian Uhlmann, Andreas Wipf, and Christian Wozar*

Theoretisch-Physikalisches Institut, Friedrich-Schiller-Universität Jena, Max-Wien-Platz 1, 07743 Jena, Germany

We consider the two-dimensional $\mathcal{N} = (2,2)$ Wess-Zumino model with a cubic superpotential at weak and intermediate couplings. Refined algorithms allow for the extraction of reliable masses in a region where perturbation theory no longer applies. We scrutinize the Nicolai improvement program which is supposed to guarantee lattice supersymmetry and compare the results for ordinary and non-standard Wilson fermions with those for SLAC derivatives. It turns out that this improvement completely fails to enhance simulations for Wilson fermions and only leads to better results for SLAC fermions. Furthermore, even without improvement terms the models with all three fermion species reproduce the correct values for the fermion masses in the continuum limit.

I. INTRODUCTION

Supersymmetric models have drawn much attention over the past decades. In particular, supersymmetric extensions of the standard model have become a primary research topic for model building. The additional symmetry of these models proves to be a very useful tool for the study of their perturbative and non-perturbative aspects. It is notoriously complicated to check and extend the predictions made by supersymmetry in a strong coupling regime where standard perturbation no longer applies.

At the same time, lattice simulations of quantum field theories have been very successful in an increasing number of applications. In some theories, it is possible to match numeric results at weak coupling to perturbative continuum results; at stronger coupling, lattice simulations are often the only viable way to investigate non-perturbative properties of the theories. As nonperturbative effects are automatically taken into account, it is desirable to apply the lattice approach also to supersymmetric theories. This has been the subject of a number of publications, see, e.g., [1, 2] and references therein. There are a number of challenges with respect to this goal since it is well known that full supersymmetry can not be realized in a generic lattice model. The reason for this can be traced back to the failure of the Leibniz rule on the lattice [3]. The full supersymmetry can only be recovered in the limit of vanishing lattice spacing (continuum limit); but only in some cases, the conditions for such a restoration are under control. E.g., it has been shown that even in supersymmetric quantum mechanics the naive discretization does not lead to a supersymmetric continuum limit [4]; generically, such a limit can at best be achieved by finetuning the bare coefficients of all supersymmetry-breaking counterterms [5]. This, however, requires much knowledge of the theory in advance. In some cases the relevant operators can be determined perturbatively, cf. [6]. A possible way beyond perturbation theory is the application of a blocking transfromation as in [7] for a free theory. This may lead to a solution similar to the Ginsparg-Wilson relation for the chiral symmetry [8].

It is possible to reduce the number of relevant operators in the continuum limit if some symmetries of the continuum theory are already realized in the lattice action. The standard lore is that it is sufficient to realize just a part of the supersymmetry on the lattice in order to ensure the correct continuum limit. There have been many suggestions and numerical investigations with respect to such a partial realization of the supersymmetry algebra on the lattice, e.g. [9] and [10]. An elegant suggestion uses a Nicolai map [11] to create lattice improvement terms that guarantee a partial realization of supersymmetry, cf. e.g. [12].

Numerical simulations of supersymmetric theories face the further difficulty that bosons and fermions on the lattice should be treated on equal footing. This demands for dynamical fermions; however, such simulations are notoriously numerically involved. Therefore, it is advisable to start with low-dimensional theories in order to gain information about the performance of the different supersymmetric lattice formulations. On the other hand, such dynamical fermion simulations in low dimensions are interesting in their own right because they allow for an explicit investigation and improvement of the corresponding known algorithms.

We have started the analysis of such low-dimensional models in a previous paper [13] with investigations of various lattice formulations of supersymmetric quantum mechanics and first tests of the two-dimensional Wess-Zumino model at weak coupling. Here we will extend the analysis of the latter theory using far more elaborate numerical techniques to reach intermediate to strong values of the coupling. We are able to simulate the Wess-Zumino model for a much larger parameter region as in related previous works [12] and [14]. Starting from the standard hybrid Monte Carlo algorithm [15] we employ a novel combination of algorithms involving both a higher-order [16] integration scheme and Fourier acceleration [17]. This entails much better statistics in combination with larger lattice sizes. These improvements lead to reliable new results even at stronger coupling where considerable deviations from perturbative predictions, e.g., for the masses of the supersymmetric partners can be observed.

A further goal was a systematic study of the effects of the above-mentioned improvement terms introduced by the Nicolai map [12]. In this paper, we present the first explicit com-

*T.Kaestner, G.Bergner, A.Wipf@tpi.uni-jena.de and S.Uhlmann, Christian.Wozar@uni-jena.de

parison of the models with and without such terms. It may come as a surprise that for Wilson fermions the "improvement term" even fails to improve the properties of the lattice model. Moreover, such terms introduce new complications and can lead to unreliable numerical results.

In previous works [13, 18] it has been demonstrated that lattice models based on the SLAC derivative [19] and on the twisted Wilson formulation (as introduced in [13]) are particularly well-behaved as far as the continuum limit is concerned. Even at large lattice spacing the continuum result is approximated very well. In the current simulation the SLAC derivative again proves to be the best choice because it allows for much larger values of the coupling constant, and only a comparably coarse lattice is needed to extract the correct continuum results. It is interesting to note that contrary to a realization with Wilson fermions the improvement terms for the SLAC derivative in fact lead to better numerical results.

The paper is organized as follows: We start out with a short introduction of the different lattice realizations of the two-dimensional $\mathcal{N} = 2$ Wess-Zumino model and the corresponding improvement terms with their respective lattice and continuum symmetries. Then, we present the numerical results of our simulations; in particular, we compare the masses of the supersymmetric partners as a measure for how well supersymmetry is realized on the lattice. A comparison of the various models with the perturbative continuum prediction at smaller values of the dimensionless coupling is the subject of Section III C. At last, we turn special attention to the regime of intermediate couplings where the measured masses differ considerably from the one-loop results.

II. LATTICE MODELS

A. Supersymmetrically improved lattice actions

The lattice models under consideration have been discussed at length in [13]. Therefore, we shall only briefly recall the definitions of the corresponding lattice actions. In terms of complex coordinates z and $\bar{z}$ for the two-dimensional Euclidean spacetime together with the corresponding holomorphic and anti-holomorphic differentials ∂ and $\bar{\partial}$ the continuum action of the $\mathcal{N} = 2$ Wess-Zumino model reads

$$S_{\text{cont}} = \int d^2x \left(2\bar{\partial}\bar{\varphi}\partial\varphi + \tfrac{1}{2}|W'(\varphi)|^2 + \bar{\psi}M\psi\right). \quad (1)$$

The bosonic potential is given by the absolute square of the derivative of the holomorphic superpotential $W(\varphi)$ w.r.t. its argument $\varphi = \varphi_1 + i\varphi_2$. Apart from the standard kinetic term for the (two-component) Dirac spinors, the Dirac operator M contains a Yukawa coupling,

$$M = \gamma^z\partial + \gamma^{\bar{z}}\bar{\partial} + W''P_+ + \overline{W}''P_-. \quad (2)$$

In (2) we have introduced chiral projectors $P_\pm = \frac{1}{2}(\mathbb{1} \pm \gamma_3)$ which in the Weyl basis with $\gamma^1 = \sigma_1, \gamma^2 = -\sigma_2, \gamma_3 = i\gamma^1\gamma^2$ project onto the upper and lower components of ψ. In the form (1) the action is invariant under four real supercharges.

Taken together they satisfy the $\mathcal{N} = (2, 2)$ superalgebra, and it has been argued that at most one supersymmetry can be preserved on the lattice [12]. With the help of the explicitly known form of the Nicolai map it is possible to construct such a lattice model straightforwardly. In terms of the Nicolai variable $\xi_x = 2(\bar{\partial}\bar{\varphi})_x + W_x$ on the lattice, the discretized Wess-Zumino action reads

$$S = \tfrac{1}{2}\sum_x \bar{\xi}_x\xi_x + \sum_{x,y} \bar{\psi}_x M_{xy}\psi_y. \quad (3)$$

Here, W_x is taken to be the lattice counterpart of the continuum operator $W'(\varphi)$, i.e. $W_x = W'(\varphi_x)$. The matrix M is given by

$$M_{xy} = \begin{pmatrix} W_{xy} & 2\bar{\partial}_{xy} \\ 2\partial_{xy} & \overline{W}_{xy} \end{pmatrix} = \begin{pmatrix} \frac{\partial\xi_x}{\partial\varphi_y} & \frac{\partial\xi_x}{\partial\bar{\varphi}_y} \\ \frac{\partial\bar{\xi}_x}{\partial\varphi_y} & \frac{\partial\bar{\xi}_x}{\partial\bar{\varphi}_y} \end{pmatrix}. \quad (4)$$

We require all lattice difference operators to be antisymmetric, $\partial_{xy} = -\partial_{yx}$. From the second equality in (4) we can read off that $W_{xy} := \partial W_x/\partial\varphi_y$.

One easily checks that (3) is invariant under the following (supersymmetry) variation,

$$\delta\varphi_x = \bar{\varepsilon}\psi_{1,x}, \quad \delta\bar{\psi}_{1,x} = -\tfrac{1}{2}\bar{\xi}_x\bar{\varepsilon}, \quad \delta\psi_{1,x} = 0, \quad (5a)$$

$$\delta\bar{\varphi}_x = \bar{\varepsilon}\psi_{2,x}, \quad \delta\bar{\psi}_{2,x} = -\tfrac{1}{2}\xi_x\bar{\varepsilon}, \quad \delta\psi_{2,x} = 0. \quad (5b)$$

In terms of the original fields, (3) takes the form

$$S = \sum_x \left(2(\bar{\partial}\bar{\varphi})_x(\partial\varphi)_x + \tfrac{1}{2}|W_x|^2 + W_x(\partial\varphi)_x + \overline{W}_x(\bar{\partial}\bar{\varphi})_x\right)$$
$$+ \sum_{x,y}(\bar{\psi}_{1,x}, \bar{\psi}_{2,x}) \begin{pmatrix} W_{xy} & 2\bar{\partial}_{xy} \\ 2\partial_{xy} & \overline{W}_{xy} \end{pmatrix} \begin{pmatrix} \psi_{1,y} \\ \psi_{2,y} \end{pmatrix}. \quad (6)$$

This supersymmetrically improved lattice action differs from a straightforward discretization of (1) by

$$\Delta S = \sum_x \left(W_x(\partial\varphi)_x + \overline{W}_x(\bar{\partial}\bar{\varphi})_x\right) \quad (7)$$

a discretization of a surface term in the continuum theory (which is therefore expected to vanish in the continuum limit for suitably chosen boundary conditions). For the free theory $(W_x = m\varphi_x)$ $\Delta S = 0$ readily follows from the antisymmetry of the difference operator ∂_{xy} while for interacting theories (7) guarantees the invariance of the action under (5) without the need of the Leibniz rule. To study the impact of SUSY improvement we will compare also the improved action with the *unimproved* straightforward discretization of (1) (without ΔS).

B. Lattice fermions

For the symmetric difference operator

$$(\partial_\mu^S)_{xy} = \tfrac{1}{2}(\delta_{x+\hat{\mu},y} - \delta_{x-\hat{\mu},y}), \quad (8)$$

doublers are inevitably introduced into both the bosonic and fermionic sector. In order to get rid of them a Wilson term may be added to the superpotential so as to maintain the invariance of the action under (5). Within this context two different choices have been discussed previously [13],

$$W_x = W'(\varphi_x) - \frac{r}{2}(\Delta\varphi)_x \qquad (9)$$

and

$$W_x = W'(\varphi_x) + \frac{ir}{2}(\Delta\varphi)_x. \qquad (10)$$

We stress that for Wilson fermions, the derivative of the superpotential is now shifted as compared to the situation after (3). From the first expression we recover the standard Wilson term for the fermions, i.e. $W_{xy} = W''(\varphi_x)\delta_{xy} - \frac{r}{2}\Delta_{xy}$. The operator Δ_{xy} is the usual two-dimensional (lattice) Laplacian $2\partial\bar{\partial}$. The second possibility (10) leads to $W_{xy} = W''(\varphi_x)\delta_{xy} + \gamma_3\frac{r}{2}\Delta_{xy}$. Here, the appearance of γ_3 motivates the name *twisted* Wilson fermions (not be confused with the recently introduced twisted mass formulation of lattice QCD). It was already shown for the free theory [13] that *twisted* Wilson fermions suffer far less from lattice artifacts than their standard Wilson cousins. Here we will show that they remain superior even for (strongly) interacting theories.

Besides these two (ultra-)local difference operators we have previously suggested to reconsider the non-local SLAC lattice derivative in the context of lattice Wess-Zumino models. The matrix elements of the SLAC derivative are most conveniently given for a one-dimensional lattice with an odd number of lattice points L,

$$\partial_{x\neq y} = (-1)^{x-y}\frac{\pi/L}{\sin(\pi(x-y)/L)}, \quad \partial_{xx} = 0. \qquad (11)$$

The generalization to higher dimensions is straightforward and amounts to forming suitable tensor products of (11).[1] For SLAC fermions no further modifications to the superpotential are necessary. It is due to this fact that they constitute an interesting alternative to Wilson fermions.

C. Discrete symmetries

For the numerical analysis of Sec. III we have chosen the superpotential

$$W(\varphi) = \tfrac{1}{2}m\varphi^2 + \tfrac{1}{3}g\varphi^3 \qquad (12)$$

which coincides with that in earlier simulations of the Wess-Zumino model [12, 14]. We will assume the coupling constants m and g to be real and positive. The superpotential (12)
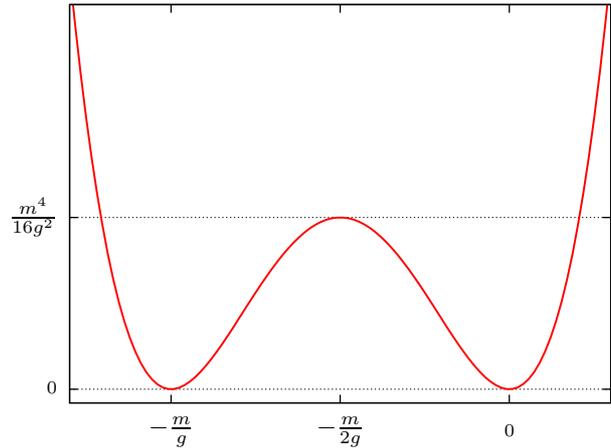
FIG. 1: Classical bosonic potential $V(\varphi) = \frac{1}{2}|W'(\varphi)|^2$ from (12) shown for vanishing imaginary part ($\varphi_2 = 0$). In the free theory limit ($g \to 0$) the left minimum is pushed towards minus infinity.

allows for discrete symmetries $\mathbb{Z}_2^R \times \mathbb{Z}_2^C$ which act as reflections interchanging the two vacua and as complex conjugations on the complex scalar field:

$$\mathbb{Z}_2^R: \varphi \mapsto -\frac{m}{g} - \varphi \quad \text{and} \quad \mathbb{Z}_2^C: \varphi \to \bar{\varphi}, \qquad (13)$$

so that also the potential $\frac{1}{2}|W'(\varphi)|^2$ is invariant under both transformations, cf. Fig. 1.

From the explicit form of the fermion matrix M and its adjoint $M^\dagger$

$$M = \gamma^\mu\partial_\mu + m + 2g(\varphi_1 + i\gamma_3\varphi_2), \qquad (14a)$$
$$M^\dagger = -\gamma^\mu\partial_\mu + m + 2g(\varphi_1 - i\gamma_3\varphi_2) \qquad (14b)$$

one finds that

$$\mathbb{Z}_2^R: M \mapsto -\gamma_3 M\gamma_3, \quad \mathbb{Z}_2^C: M \mapsto \gamma_3 M^\dagger\gamma_3, \qquad (15)$$

which shows the invariance of the determinant.[2]

Apart from Lorentz transformation, the continuum model is (irrespectively of the concrete form of the superpotential) also invariant under time reversal and parity transformations

$$\mathbb{Z}_2^T: (z, \bar{z}) \mapsto (-\bar{z}, -z), \quad \mathbb{Z}_2^P: (z, \bar{z}) \mapsto (\bar{z}, z). \qquad (16)$$

Barring possible Wilson terms, the unimproved lattice models obviously inherit all discrete symmetries from the continuum. By contrast, the supersymmetrically improved lattice models are invariant only under a combination of all symmetries. We find

$$\mathbb{Z}_2^R: W'_x(\partial\varphi)_x \mapsto -W'_x(\partial\varphi)_x, \qquad (17a)$$
$$\mathbb{Z}_2^C: W'_x(\partial\varphi)_x \mapsto \overline{W}'_x(\partial\bar{\varphi})_x. \qquad (17b)$$

---

[1] The reason for an odd number of lattice points originates from a reality condition on the matrix elements (11). As such it is a mere technicality in order to ease numerical simulations.

[2] This is true at least up to an irrelevant sign. On the lattice the fermion matrix M always has an even number of rows and columns, hence this phase does not appear.

TABLE I: Comparison of various lattice models w.r.t. their symmetries. All statements refer to to the interacting theory, i.e. $g \neq 0$. The notion $\mathbb{Z}_2^{\mathrm{PC}}$ denotes the combined action of a field and parity transformation as discussed in the text.

	(1) Wilson impr.	(2) Wilson unimpr.	(3) twisted Wilson[a]	(4) SLAC impr.	(5) SLAC unimpr.
lattice derivative	local	local	local	non-local	non-local
lattice artifacts	$\mathcal{O}(a)$	$\mathcal{O}(a)$	$\mathcal{O}(a)^b$	'perfect'	'perfect'^{c}
modifications to superpot.	yes	yes	yes	no	no
discrete symmetries	$\mathbb{Z}_2^{\mathrm{PC}}$	$\mathbb{Z}_2^{\mathrm{T}} \times \mathbb{Z}_2^{\mathrm{P}} \times \mathbb{Z}_2^{\mathrm{C}}$	$\mathbb{Z}_2^{\mathrm{TR}}$	$\mathbb{Z}_2^{\mathrm{TPR}} \times \mathbb{Z}_2^{\mathrm{PC}}$	$\mathbb{Z}_2^{\mathrm{T}} \times \mathbb{Z}_2^{\mathrm{P}} \times \mathbb{Z}_2^{\mathrm{R}} \times \mathbb{Z}_2^{\mathrm{C}}$
supersymmetries	one	none	one	one	none

^{a}Only improved considered.

^{b}In the interacting case the good scaling properties are lost. However the overall size of lattice artifacts is still much smaller when compared to Wilson fermions.

^{c}The dispersion relation is up to the cut-off the same as in the continuum.

Thus, for the improved models (with SLAC fermions) the continuum symmetry is reduced,

$$\mathbb{Z}_2^{\mathrm{T}} \times \mathbb{Z}_2^{\mathrm{P}} \times \mathbb{Z}_2^{\mathrm{R}} \times \mathbb{Z}_2^{\mathrm{C}} \longrightarrow$$
$$\mathbb{Z}_2^{\mathrm{TPR}} \times \mathbb{Z}_2^{\mathrm{PC}} := \mathrm{diag}(\mathbb{Z}_2^{\mathrm{T}} \times \mathbb{Z}_2^{\mathrm{P}} \times \mathbb{Z}_2^{\mathrm{R}}) \times \mathrm{diag}(\mathbb{Z}_2^{\mathrm{P}} \times \mathbb{Z}_2^{\mathrm{C}}). \quad (18)$$

Here, the diagonal subgroup $\mathrm{diag}(\mathbb{Z}_2^{\mathrm{P}} \times \mathbb{Z}_2^{\mathrm{C}})$ is a group $\mathbb{Z}_2^{\mathrm{PC}}$ generated by the product of the generators of $\mathbb{Z}_2^{\mathrm{P}}$ and $\mathbb{Z}_2^{\mathrm{C}}$ (analogous notations are used for the other groups). It readily follows that the improvement term must have a vanishing expectation value in the original ensemble without improvement. We have checked this with a large numerical precision. For Wilson and twisted Wilson fermions with improvement the r. h. s. of (18) is even further broken down due to the presence of the (twisted) Wilson term in the superpotential. For Wilson fermions, the bosonic action can be read off from (6) and (9),

$$S_{\mathrm{B}} = \tfrac{1}{2} \sum_x \left| (\bar{\partial}\bar{\varphi})_x + W'_x - \tfrac{r}{2}(\Delta\varphi)_x \right|^2. \quad (19)$$

Since Δ_{xy} is invariant under both time reversal and parity, (17) cannot be preserved; the Wilson term inevitably changes sign. Conversely, from the bosonic action with twisted Wilson fermions

$$S_{\mathrm{B}} = \tfrac{1}{2} \sum_x \left| (\bar{\partial}\bar{\varphi})_x + W'_x + \tfrac{ir}{2}(\Delta\varphi)_x \right|^2. \quad (20)$$

only $(\varphi \to -m/g - \bar{\varphi}, \partial \to -\bar{\partial})$ can be shown to yield a symmetry. In either case the breaking of the other symmetries is induced by a higher-dimensional operator and may be expected to be at most $\mathcal{O}(a)$ [12, 20]. Nevertheless, at finite lattice spacing, the physics might be affected since the overall size of the breaking terms is a dynamical question. By contrast, SLAC fermions with the larger symmetry (17) are again favored.

In Tab. I we summarize all lattice models to be dealt with in the next section.

III. NUMERICAL RESULTS

As outlined in the introduction we have employed the standard hybrid Monte Carlo algorithm for our numerical simulations. The fermion determinant was estimated stochastically utilizing real pseudo-fermion fields. The reason for real pseudo-fermions derives from the presence of only a single flavor such that the square root of the pseudofermionic kernel $Q^{-1} = (MM^T)^{-1}$ is actually needed. We note in passing that the pseudo fermion action remains real with this choice since also the fermion matrix is real for Majorana basis is chosen. Hence the latter was adopted for all our simulations. A significant gain was achieved by combining higher order integrators with Fourier acceleration techniques. With the help of the former one can avoid the requirement for ever smaller time-step sizes during the MD step of the HMC while a careful tuning of the latter allows for autocorrelation times $\tau \leq 5$ over the whole range of parameters analysed. In particular for small lattice spacings, i.e. at large lattice sizes this was seen to reduce significantly critical slowing down as also reported in [21]. A detailed account of the algorithm employed here will be published separately at a later time.

A. Dynamical properties of improved lattice actions

Before discussing measurements of physical observables in the next section we will first focus on the improvement term (7). The aim is to understand the difference between improved and unimproved lattice models w.r.t. predictions of supersymmetry. One possible test is a measurement of the bosonic action itself. With the help of the Nicolai map appearing in (3) one can show that

$$\langle S_{\mathrm{B}} \rangle = N. \quad (21)$$

Here, $N = N_{\mathrm{t}} \times N_{\mathrm{s}}$ denotes the total number of lattice points, and (21) is only expected to hold when fermions are included dynamically. Then, however, this prediction holds irrespectively of the concrete value of the coupling constants. With a slightly different argument the same was also found in [12].
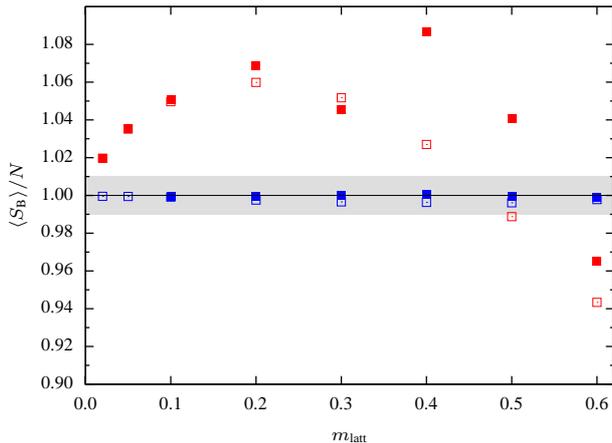
FIG. 2: Normalized bosonic action as a function of the bare mass lattice parameters using Wilson fermions with the improved (filled squares) and unimproved (empty squares) actions from either quenched (red) or dynamical fermion (blue) simulations ($N = 16 \times 16$).
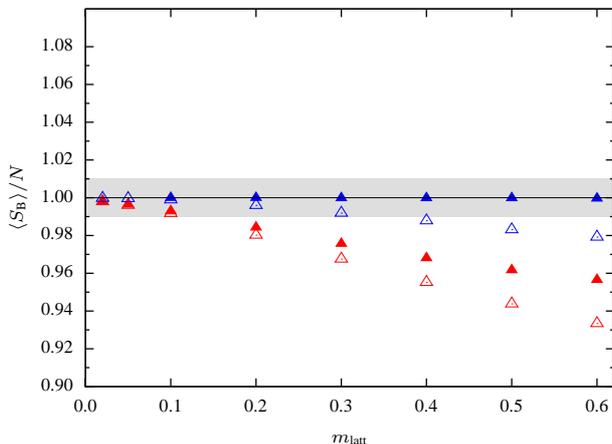
FIG. 3: Same as in Fig. 2 but for SLAC fermions.

Equation (21) provides a test observable distinguishing improved from unimproved lattice models as well as quenched from dynamical fermion simulations. To accomplish this, we have run simulations with both (standard) Wilson and SLAC fermions. The results are shown as a function of the bare lattice mass parameter $m_{\text{latt}} = m/N_s$. Since the continuum limit for this theory is obtained from $m_{\text{latt}} \to 0$, smaller values of m_{latt} likewise mean a finer lattice spacing (and for fixed N a smaller spacetime volume). The dimensionless coupling strength $\lambda = g/m$ was set to $\lambda = 1$. The lattice sizes we used for our numerical simulations were $N = 16 \times 16$ for Wilson and $N = 15 \times 15$ for SLAC fermions. For the quenched simulations 500,000 (independent) configurations were evaluated, and 30,000 configurations with dynamical fermions were analysed. The results are shown in Fig. 2 for Wilson and in Fig. 3 for SLAC fermions. One clearly observes that the quenched data significantly deviate from the predicted value which illustrates the necessity of dynamical
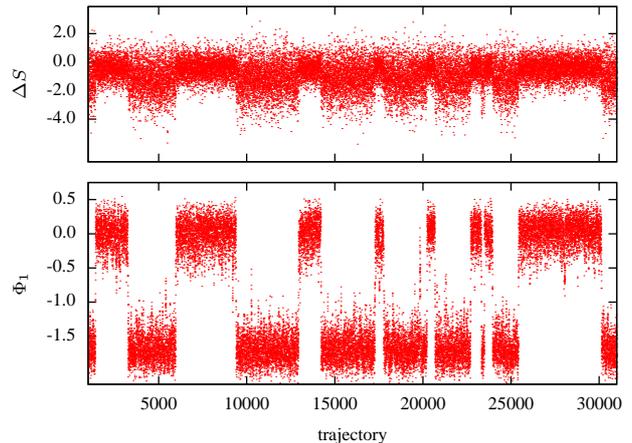
FIG. 4: MC history of the lattice mean $\Phi_1 = N^{-1} \sum_x \varphi_{1,x}$ and size of the improvement term for Wilson fermions ($N = 16 \times 16$, $\lambda = 0.6$, $m_{\text{latt}} = 0.3$).

fermion contributions in order to retain supersymmetry. Using an unimproved action with dynamical fermions we find much smaller deviations which in case of the Wilson fermions are already hard to distinguish from the improved results. For SLAC fermions the deviations are somewhat more systematic and remain also clearly distinguishable from other dynamical fermion simulations. A second difference between Wilson and SLAC fermions may be infered from Fig. 4. Namely, there is a distinct correlation between the ground state around which the field φ_1 fluctuates on the one hand and size and variance of the improvement term on the other hand. This may be taken as direct manifestation of the additionally broken $\mathbb{Z}_2^{\text{TPR}}$-symmetry due to the Wilson term which will also play a role when discussing the failure of improvement in the next paragraphs.

Limitations of improved lattice actions

Studying the improvement term ΔS for models with either Wilson or SLAC fermions we have found that the system is ultimately pushed into an unphysical region of configuration space, at least for strong coupling. Our simulations have revealed that this instability is controlled by the actual size of the bare mass parameter and the coupling strength λ. Simulations tend to fail more often as either of them grows. The study of this phenomenon with Wilson fermions turns out to be clumsy since there is no clear correlation between the value of the coupling and the number of configurations where the instability occurs. Hence we prefer to present our analysis from the simulations with SLAC fermions. However, it should be emphasized again that for either Wilson or twisted Wilson fermions the qualitative picture is the same as described below.

It is to be expected that the improvement term grows with the coupling strength λ and vanishes continuously in the continuum limit (at $m_{\text{latt}} = 0$). We observe a good scaling behavior w.r.t. the lattice size, see also Fig. 5. For all couplings
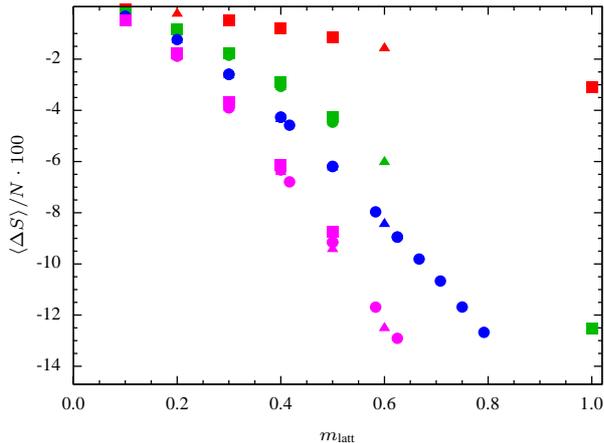
FIG. 5: Reduced improvement term $\Delta S/N$ for different lattice sizes: 9×9 (squares), 15×15 (triangles) and 25×25 (circles). Colors depict $\lambda = 0.8$ (red), 1.0 (green), 1.2 (blue), 1.5 (magenta).

FIG. 6: MC history of improvement term and fermion determinant (SLAC improved, $N = 15 \times 15$, $m_\text{latt} = 0.6$, $\lambda = 1.4$ (green), 1.7 (red), 1.9 (blue)).

FIG. 7: MC history of normalized lattice mean $\Phi_1 g/m$ (SLAC impr., $N = 15 \times 15$, $m_\text{latt} = 0.6$, $\lambda = 1.4$ (green), 1.7 (red), 1.9 (blue)).

FIG. 8: Mode analysis of ensembles in the physical (green, $\lambda = 1.4$) and unphysical (red, $\lambda = 1.7$) phase. Here ρ is the distribution function for the modulus of the lattice momentum averaged over 25,000 configurations (SLAC improved, $N = 15 \times 15$, $m_\text{latt} = 0.6$).

λ and m_latt the improvement term is found to be smaller than 14% of the total bosonic action. Depending on the coupling strength λ, this ratio is reached sooner or later. Actually, this represents a threshold above which the simulation fails. The situation is depicted in Figs. 6 and 7. At some instant, the improvement term blows up and settles again at a value about 40 times the size of the bosonic action. At the same time also the fermion determinant grows drastically and so hinders the system from returning into the original (and desired) region of configuration space. A reason for this instability may be found by reconsidering the improved action

$$S_\text{B} = \frac{1}{2} \sum_x \left| 2(\partial\varphi)_x + \overline{W}_x \right|^2. \tag{22}$$

In this form the action allows for two distinct behaviors of the fluctuating fields. The physically expected behavior consists of small fluctuations around the classical minima of the potential. Alternatively, (22) allows for large fluctuations of φ to be compensated by large values of $\overline{W}_x$. The latter would be dominated by UV contributions, and this is what we actually observe, cf. Fig. 8. In this situation, it is definitely no longer possible to extract meaningful physics. Another view on this "broken" phase is taken in Fig. 7. While the ensemble with $\lambda = 1.4$ exhibits the expected behavior at the only slightly larger value of $\lambda = 1.7$ the simulation breaks down after about 5,000 configurations and for $\lambda = 1.9$ the simulation is instantly found in the broken phase.

To sum up, we have observed that the improved lattice models may become unstable at any finite m_latt and hence any finite lattice spacing. If and when this happens depends on several factors. Wilson fermions are affected in a stronger way while SLAC fermions remain stable for a much wider range of coupling constants. Apart from that, one should ensure by monitoring the improvement term or any other observable discussed above explicitly that a simulation is not subject to this phenomenon. For the practitioner this is of course a major nuisance and possibilities to avoid this matter are already under
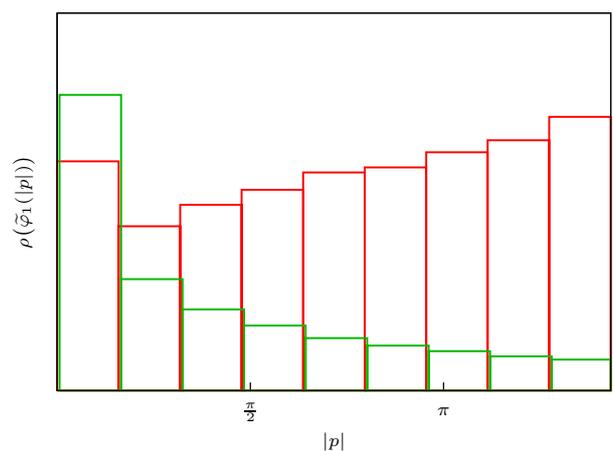
investigation. Provided that one is confined to lattices smaller than 64×64 but demands the absence of finite-size effects, improved lattice models with Wilson fermions can be used for the continuum extrapolation of masses only up to $\lambda < 0.4$. SLAC fermions can be used in the greater range of $\lambda < 1.5$; the corresponding results will be presented further below.

B. Setting the stage

In Monte-Carlo simulations, importance sampling is only meaningful with respect to a positive measure. However, including dynamical fermions the measure is $\det(M) \exp(-S_{\mathrm{B}})$. While the exponential factor is strictly positive (S_{B} is real), the positivity of the determinant cannot be guaranteed for an interacting theory and a possibly emerging sign problem has to be addressed. In order to make sensible comparisons with continuum calculations (which are most conveniently performed in an infinite spacetime) one furthermore must make sure that physical observables extracted from lattice simulations are free of finite-size effects. In order to check this, all simulations in this section are repeated in portions of fractional volume l^2 of a fixed physical unit volume (with various values for $l = N_{\mathrm{s}}a$ on a square lattice with $N = N_{\mathrm{t}} \times N_{\mathrm{s}}$ lattice points). In the following we consider both issues in more detail.

1. Negative fermion determinants

The Nicolai map in a supersymmetric theory is a change of bosonic variables which renders the bosonic part of the action Gaussian; at the same time, the Jacobian of this change of variables has to cancel the fermion determinant. In our model, this means

$$\det(M) = \det\left(\frac{\delta}{\delta\varphi} \big(2(\bar{\partial}\bar{\varphi}) + W' \big) \right). \qquad (23)$$

In this light, an indefinite fermion determinant obviously corresponds to a non-invertible change of variables in the continuum,

$$\varphi \mapsto \xi = 2\bar{\partial}\bar{\varphi} + W'. \qquad (24)$$

This map is only globally invertible if the superpotential is of degree 1 (the Nicolai map in this case has winding number 1), i.e., for the free theory [22]. For our choice $W'(\varphi) = m\varphi + g\varphi^2$ the map is not *globally* invertible, and there exists at least one point where $\det(M)$ vanishes iff $g \neq 0$. By this line of argument (for the continuum formulation of the model) negative determinants cannot be ruled out.

One way to cope with this in practical simulations is to use $|\det(M)| \exp(-S_{\mathrm{B}})$ for the generation of configurations instead and to reweigh with the sign afterwards. Unfortunately, calculating the sign of $\det M$ is as costly as the computation of the whole determinant. Hence, this method becomes unfeasible for large lattices. A way out is to avoid reweighing
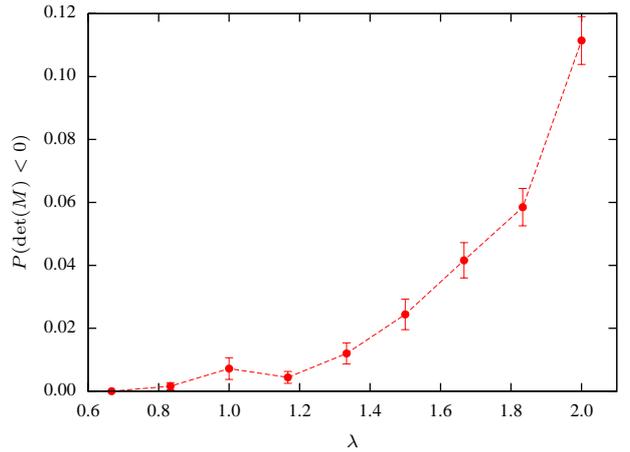
FIG. 9: Probability for negative determinants (Wilson unimproved, $N = 14 \times 14$, $m_{\mathrm{latt}} = 0.43$).
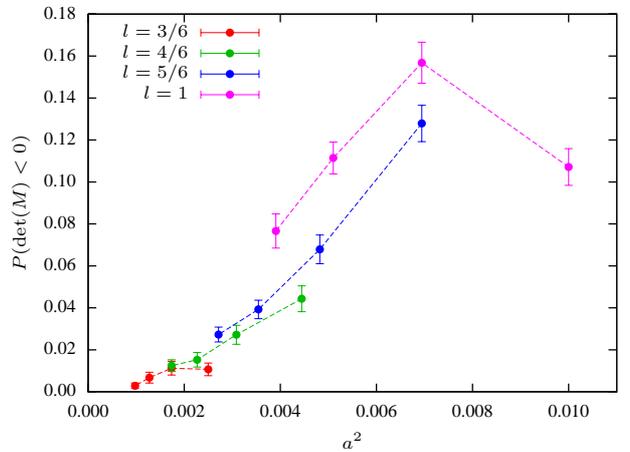
FIG. 10: Probability for negative determinants at different box sizes with varying lattice size (Wilson unimproved, $m = 6$, $\lambda = 2.0$).

within certain bounds for the parameters in which the ensuing systematic errors are negligible. Thus, we have to estimate the frequency of occurrence of negative determinants as a function of the parameters. To obtain more reliable results we have studied this subject with a naive inversion algorithm which computes the determinant from a LU decomposition and takes its contributions exactly into account. This is numerically much more involved than the standard pseudofermion algorithm, thus, this method is only applicable to small lattice sizes with up to 16×16 lattice sites. For fixed physical mass m it can be gleaned from Fig. 9 that configurations with a negative sign of the determinant show up only for $\lambda > 1.0$. Furthermore, in order to understand the dependence on the lattice size and the lattice spacing we have fixed the coupling to $\lambda = 2.0$ and run simulations on fractions l^2 of a unit physical volume ($l \in \{3/6, 4/6, 5/6, 6/6\}$) and different lattice spacings. The results displayed in Fig. 10 clearly show that the problem dissolves in the continuum limit but becomes worse at every finite lattice spacing when the physical volume is increased. For both figures, for each data point

about 50,000 configurations were evaluated. Eventually, to estimate the impact on actual measurements we have measured the bosonic action with $m = 5$, $\lambda = 2$ on a 12×12 lattice and obtained about 7% configurations with a negative sign for the fermion determinant. The expectation values considered here are $\langle S_B \rangle_{\text{non-reweighed}} = 149.94(12)$ and $\langle S_B \rangle_{\text{reweighed}} = 149.49(10)$. Hence even at large coupling (far larger than what we target at in the next section) effects may be assumed to be at most of marginal relevance for actual measurements.

2. Finite size effects

For these models the bare mass m_{latt} also sets the scale for the overall spacetime volume. As with all lattice simulations we have to balance finite-size and discretization errors. If the lattice spacing is chosen too large, lattice artifacts may grow; on the other hand if, say, the Compton wavelength of a particle is larger than the spacetime volume the extraction of masses may suffer from finite-size effects. One way to test for the presence of such finite-size violations is to study the model at different spacetime volumes. Comparing the fermion species introduced earlier Wilson fermions may be expected to be most affected. Here, lattice artifacts further increase the correlation lengths so that measurements are much more sensitive to the finite box size. Our setup for this analysis is as follows. At first we have simulated the improved lattice model using Wilson fermions at fixed coupling parameters $m = 15$ and $\lambda = 0.3$ for five different lattices with $N_t = N_s \in \{20, 24, 32, 48, 64\}$ lattice points in each direction ($N = N_t \times N_s$). In the following we assume that with this choice of coupling constants the spacetime volume is large enough so as to allow for a sufficiently good identification with the thermodynamic limit. The masses obtained from these simulations were extrapolated to the continuum as described in App. B. This is also shown in Fig. 11 where the resulting fit (and its uncertainty) is depicted with a gray shaded area. The next step is to decrease the volume to fractions l^2 (with $l \in \{9/15, 7/15, 5/15, 3/15\}$) of a fixed physical unit volume. As long as no finite-size effects are visible we expect to find the masses extracted at these smaller and smaller volumes to lie on top of the fit from the original lattice (of unit volume). Up to a volume less than half the size of the original one this scaling may be easily infered from Fig. 11 which justifies a posteriori the correctness of our earlier assumption.

However, since by perturbation theory the physical masses decrease for growing coupling (see next section), we expect growing Compton wavelengths and therefore stick to unit volume ($l = 1$) for all further measurements so as to exclude finite-size effects.

C. Weak coupling

An interesting observable for comparing lattice results with continuum physics is the mass of the lightest excited state, i.e.
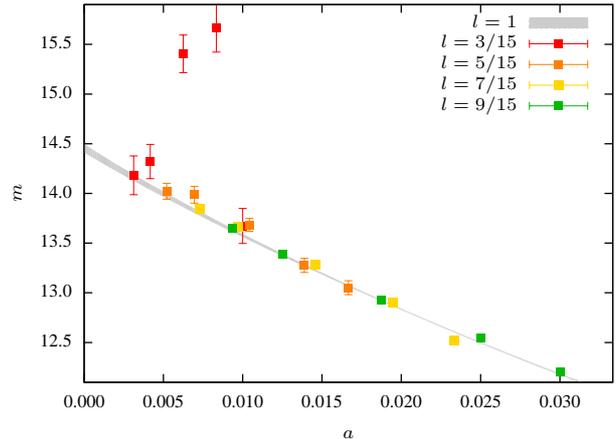
FIG. 11: Lattice masses for $m = 15$, $\lambda = 0.3$ on box sizes $l \in [0.2, 0.6]$. We see a systematic deviation from the $l = 1$ result below $l \approx 0.5$.

the energy gap. Since unbroken supersymmetry in the continuum predicts that bosonic and fermionic masses coincide it also provides a possibility to check the supersymmetric properties of the lattice prescription. The corresponding values can be extrapolated from the lattice masses in the continuum limit. In the weak coupling it will be possible to match these results to predictions of perturbation theory. This provides an important test for the numerical results and ensures that also the results at intermediate coupling are reliable.

For a description of our prescription for the boson and fermion mass extraction from correlators on the lattice we refer the interested reader to App. A. With these methods we are aiming at a test of the lattice results against perturbation theory for $\lambda \leq 0.3$.

The reference value is given by a one-loop calculation of the renormalized mass

$$m_{\text{ren}}^2 = m \left(1 - \frac{4\lambda^2}{3\sqrt{3}}\right) + \mathcal{O}(\lambda^4) \qquad (25)$$

in the continuum valid for $\lambda \ll 1$ with the bare mass m as used in Eq. (12). To obtain this result one first must calculate contributions of the loop diagrams to the propagator. An expansion in λ then yields the above result.[3]

As will be show below the fermionic masses have lower statistical errors than the bosonic ones. Therefore we compare only the extrapolations for fermionic masses to the perturbative results. This procedure gets justified by the fact that bosonic and fermionic masses coincide even on a finite lattice for the weak coupling regime as described below in Sec. III C 3.

---

[3] We will elaborate on the analytical side and the determination of the effective potential of this theory in a forthcoming publication.
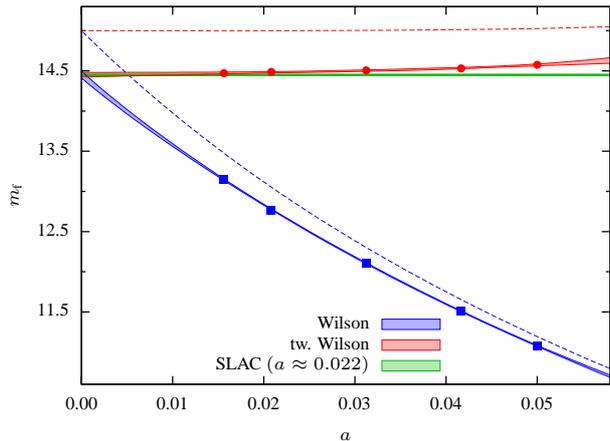
FIG. 12: The continuum extrapolation of masses for $\lambda = 0.3$ for the improved Wilson and twisted Wilson model. Here, the SLAC result is given for one single lattice size. For comparison the exact results for the free theory are also shown.

1. Continuum limit

The methods to extrapolate to the continuum given in App. B are based on the free theory with $\lambda = 0$. Since we are interested in the interacting case we must first make sure that the continuum extrapolation of masses remains stable even for $\lambda = 0.3$.

To that purpose we consider the masses in the improved model with standard Wilson and twisted Wilson fermions at $\lambda = 0.3$ at different lattice spacings a. In the perturbative coupling regime we use throughout square lattices of sizes $N_t = N_s \in \{20, 24, 32, 48, 64\}$. These correspond to lattice spacings of about $a \in [0.015625, 0.05]$. A statistics of 10,000 independent configurations puts us in a position to extrapolate to the continuum.

Using these masses $m(a)$ at finite lattice spacing the extrapolation is shown in Fig. 12. For comparison we also mark the mass for SLAC fermions at a finite lattice size $N_t = N_s = 45$ (corresponding to $a \approx 0.022$). All these results indicate that even at $\lambda = 0.3$ the continuum extrapolated masses coincide within error bounds. Even better, the masses of SLAC fermions at finite lattice spacing can not be distinguished from the continuum result.

2. Comparison with perturbation theory

As described above we extrapolate masses for Wilson (improved and unimproved) and twisted Wilson (improved) fermions for $\lambda \in [0, 0.3]$ to the continuum values, cf. Fig. 13. The masses coincide within error bars although the twisted Wilson masses are systematically smaller. This difference has to be interpreted as a systematic error in the continuum extrapolation for the masses but its effect is almost overshadowed by the statistical errors in our case. However this result indicates that for a reliable extrapolation at larger statistics finer lattices
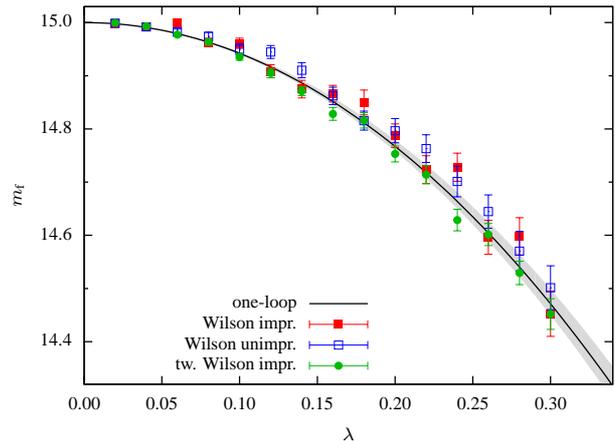
FIG. 13: Continuum masses for the weakly coupled regime in comparison to the perturbative result. The shaded area corresponds to the extrapolation provided by the continuum results according to Eq. (26) with $m = 15$ and $b = 1.35(13)$.

TABLE II: Continuum extrapolations of fermionic masses for Wilson and twisted Wilson fermions in the weak coupling regime.

λ	Wilson unimp.	Wilson imp.	tw. Wilson
0.02	14.999(2)	14.997(2)	14.999(1)
0.04	14.992(4)	14.993(4)	14.993(3)
0.06	14.982(6)	14.999(7)	14.977(4)
0.08	14.974(8)	14.963(8)	14.963(5)
0.10	14.95(1)	14.96(1)	14.935(6)
0.12	14.94(1)	14.91(1)	14.905(9)
0.14	14.91(1)	14.87(2)	14.871(9)
0.16	14.86(2)	14.87(2)	14.83(1)
0.18	14.82(2)	14.85(2)	14.82(1)
0.20	14.80(2)	14.79(2)	14.75(2)
0.22	14.76(3)	14.72(3)	14.71(2)
0.24	14.70(3)	14.73(3)	14.63(2)
0.26	14.64(3)	14.60(3)	14.60(2)
0.28	14.57(4)	14.60(4)	14.53(2)
0.30	14.50(4)	14.45(4)	14.45(3)

can be necessary to yield a better continuum limit.

As a further test we use these results to reproduce the perturbative formula

$$m(\lambda) \approx m_0 \sqrt{1 - \frac{\lambda^2}{b}}. \qquad (26)$$

Taken this functional form for granted, the parameters m_0 and b can be extracted from a least-square fit to the given data. For this fit we can use our knowledge about the free theory ($m_0 = 15$) as a fixed input or, alternatively, allow for both m_0 and b as free parameters. The corresponding results are given in Tab. III.

The extrapolated results for m_0 confirm that the extrapolation to the free theory works reliably and that we can expect

TABLE III: Fit for the perturbative mass formula with $\mathcal{O}(\lambda^2)$ corrections to be compared with the one-loop results. For comparison the one-loop result is $b \approx 1.2990$.

derivative	b	m_0
Wilson improved	1.34(6)	15.007(6)
Wilson unimproved	1.39(7)	15.008(6)
twisted Wilson improved	1.26(4)	14.996(4)
Wilson improved	1.37(5)	fixed to 15
Wilson unimproved	1.42(6)	fixed to 15
twisted Wilson improved	1.25(3)	fixed to 15

to obtain meaningful results for b. Furthermore the results obtained for improved and unimproved Wilson fermions coincide very well and therefore both provide the correct continuum limit.

Additionally the results for standard Wilson and twisted Wilson fermions lead to compatible results when taking systematic uncertainties of the continuum extrapolation into account.

As an important result of these observations, all three models considered in the weak coupling case tend towards the same continuum limit for $\lambda > 0$. The perturbative results can be recovered where the largest error bars (including possible systematic errors) yield $b = 1.35(13)$ in agreement with the one-loop result of $b_{\text{one-loop}} \approx 1.2990$.

3. Signs of supersymmetry at finite lattice spacing

Apart from all results solely based on fermions, we are primarily interested in the restoration of supersymmetry on the lattice. For this reason we better also check the demand from supersymmetry that the masses of bosonic and fermionic superpartners match. This is going to be checked by computing bosonic and fermionic masses at couplings $\lambda = 0.2$ and $\lambda = 0.4$ with $m = 15$ for all the models on different lattice sizes.

As we have seen in the whole weak coupling regime the fermionic masses do not suffer from statistical noise. This behavior derives from the fact that the fermionic correlator for the free theory ($\lambda = 0$) is independent of the bosonic field φ and is obtained by a pure matrix inversion. At small (and finite) λ, corrections to the free propagator are of $\mathcal{O}(\lambda^2)$, and the fluctuations of φ during the simulation are suppressed with λ^2; a statistics of only 10^4 is needed to get reliable results.

On the other hand the bosonic correlator even for the free theory is given by the correlations of the fluctuating field φ. Therefore a much higher statistics is necessary to sample the bosonic two-point function. Here, problems arise by the exponentially growing relative error of the two-point function $C(t)$ with respect to t.

Only with the use of an algorithm combining Fourier acceleration with higher order integrators it was possible to simulate 10^6 to 10^7 configurations for each parameter set (m, λ) with an autocorrelation time of the two-point function of

TABLE IV: For different models and lattice sizes we computed bosonic and fermionic masses with bare mass $m = 15$.

model	N_{s}	λ	m_{f}	$m_{\text{b,1}}$	$m_{\text{b,2}}$
Wilson impr.	24	0.2	11.592(2)	11.53(4)	11.59(4)
	24	0.4	11.375(4)	11.39(3)	11.34(3)
	32	0.2	12.224(2)	12.20(3)	12.15(4)
	32	0.4	11.945(5)	11.95(3)	11.88(4)
	48	0.2	12.941(5)	12.87(5)	13.02(5)
	48	0.4	12.548(13)	12.47(4)	12.53(4)
	64	0.2	13.349(10)	13.45(9)	13.32(9)
	64	0.4	12.89(3)	12.73(9)	12.83(9)
Wilson unimpr.	24	0.2	11.591(2)	11.58(2)	11.63(3)
	24	0.4	11.400(4)	11.44(2)	11.39(3)
	32	0.2	12.221(2)	12.20(3)	12.15(4)
	32	0.4	11.965(5)	11.97(3)	11.87(4)
	48	0.2	12.942(5)	12.92(6)	13.00(7)
	48	0.4	12.572(14)	12.54(4)	12.49(4)
	64	0.2	13.347(7)	13.45(9)	13.32(9)
	64	0.4	12.91(2)	12.82(9)	12.79(9)
tw. Wilson (impr.)	24	0.2	14.811(7)	14.94(11)	14.91(12)
	24	0.4	14.13(1)	14.21(9)	14.06(8)
	32	0.2	14.788(6)	14.61(14)	14.94(12)
	32	0.4	14.08(1)	14.39(14)	13.68(13)
	48	0.2	14.789(6)	14.74(11)	14.61(11)
	48	0.4	14.04(1)	14.16(16)	13.98(15)
SLAC impr.	45	0.2	14.768(4)	14.87(10)	14.83(9)
	45	0.4	13.997(13)	14.08(11)	13.92(10)
SLAC unimpr.	45	0.2	14.769(4)	14.75(6)	14.57(6)
	45	0.4	14.047(16)	13.74(8)	13.75(7)

$\tau \leq 2$.

The results of these numerical efforts are summarized in Tab. IV. They show that independently of the model even for $\lambda \in \{0.2, 0.4\}$ bosonic and fermionic masses correspond to each other and lattice-induced supersymmetry breaking can not be observed.

Finally in Figs. 14 and 15 the derived bosonic and fermionic masses are shown for the improved (and unimproved) model with Wilson fermions. Even these high statistics do not allow for a clear cut distinction between the extrapolated continuum masses of bosons and fermions for the improved and the unimproved models. This proves that even at $\lambda = 0.4$ the improvement is not necessary even on a finite lattice. Each model tends towards the supersymmetric continuum limit.

D. Intermediate coupling results

Earlier attempts to go beyond the perturbative regime could not reliably determine the mass spectrum. Namely, this was hindered by instabilities introduced by improvement terms. For Wilson fermions, this renders simulations at intermediate couplings invalid. For our analysis of coupling constants
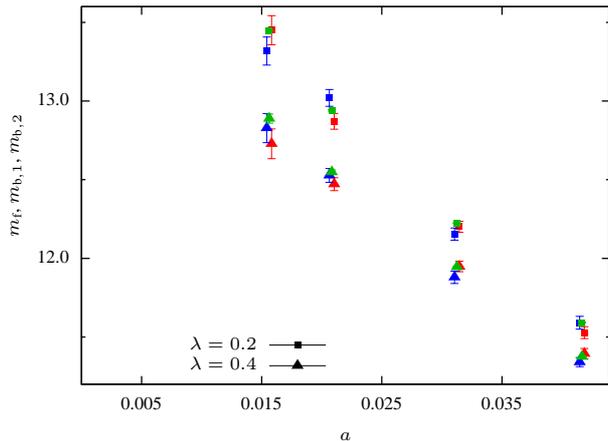
FIG. 14: Bosonic and fermionic masses for the weakly coupled regime for the improved Wilson model.
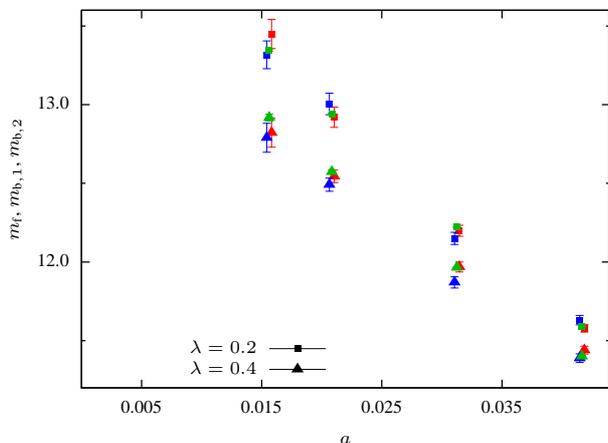
FIG. 15: Bosonic and fermionic masses for the weakly coupled regime for the unimproved Wilson model.

in the intermediate regime ($0.3 < \lambda \leq 1.2$) we have therefore only considered actions with twisted Wilson and SLAC fermions (which are anyhow expected to give better results at finite lattice spacing). For twisted Wilson fermions we have run simulations with the improved action on lattices with $N_{\mathrm{s}} \in \{32, 40, 48, 56, 64\}$ lattice points in the spatial direction. For the temporal direction we have used $1.25 \cdot N_{\mathrm{s}}$ lattice points in order to be able to assess whether contributions from higher excited states are really absent. At the chosen value of $m = 15$ in all simulations, the respective bare lattice mass parameter m_{latt} confines the attainable coupling strengths to $\lambda \leq 0.7$.[4] For even larger coupling strengths λ only SLAC fermions have been found to yield sensible results. In our simulations we used for this species both the improved and unimproved lattice models on a fixed lattice size of $N = 45 \times 45$.

TABLE V: Fermionic masses for the intermediate coupling case. Twisted Wilson results are continuum extrapolations whereas the SLAC data is from a 45×45 lattice.

λ	tw. Wilson	SLAC unimp.	SLAC imp.
0.20	14.80(2)	14.769(4)	14.768(4)
0.35	14.23(2)		
0.40	13.99(3)	14.05(2)	14.00(1)
0.45	13.62(5)		
0.50	13.30(6)		
0.55	12.8(1)		
0.60	12.2(1)	12.81(4)	12.44(6)
0.65	11.9(2)		
0.70	10.4(5)		
0.80		11.49(9)	10.2(3)
1.00		10.2(2)	9.4(2)
1.20		10.1(3)	9.1(3)

Apart from that, one further run was done on a 63×63 lattice with $\lambda = 0.8$. Square lattices turned out to be more convenient with SLAC fermions and to be sufficient to clearly read off (within statistical errors) the masses. As for the simulations with twisted Wilson fermions we have determined only the masses from the fermionic correlators since with the statistics (50,000 trajectories) achieved so far the bosonic correlators are far too noisy to yield reliable results.

Our results may be found in Tab. V and are depicted graphically in Fig. 16. From the comparison with perturbation theory first deviations are seen as soon as $\lambda \geq 0.4$ where the (extrapolated) lattice results are slightly stronger curved. Also clear deviations between the improved and unimproved model using SLAC fermions become apparent for $\lambda \geq 0.6$. It is worthwhile to note that the result from the improved lattice model is closer to the continuum limit which may be infered
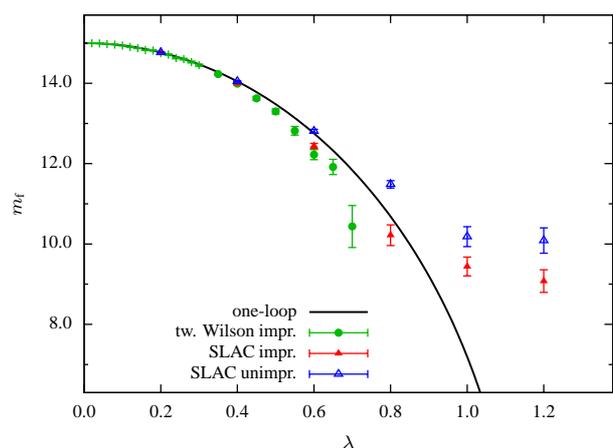
FIG. 16: Masses of the improved and unimproved model with SLAC fermions on a 45×45 lattice and continuum extrapolated results for twisted Wilson fermions are compared with the perturbative one-loop result in the continuum.

---

[4] For $\lambda = 0.7$ we already observed that the simulation failed on the coarsest lattice and had to be excluded.

TABLE VI: Fermionic masses for the SLAC derivative on two different lattice sizes for $\lambda = 0.8$.

N_s	improved	unimproved
45	10.22(26)	11.49(9)
63	10.54(15)	10.70(19)

from Tab. VI. While the lattice data from the improved model almost coincide for both lattice spacings the data from the unimproved model is likely to approach the same value if increasingly finer grained lattices are used.

Larger values of λ are attainable however the numerical effort becomes more involved and some technicalities need to be addressed. Once this is under control we are confident to investigate the strong coupling regime with the improved models up to $\lambda = 2.0$ on the same lattice sizes. The interesting question whether the masses of superpartners still agree can then be satisfactorily answered.

IV. CONCLUSIONS AND OUTLOOK

In this article we have presented a detailed numerical analysis of the two-dimensional $\mathcal{N} = (2, 2)$ Wess-Zumino model. Due to algorithmic improvements we were able to study lattice models at much larger lattice sizes, i.e. smaller lattice spacings and more importantly at stronger couplings. For a comparison with analytical results from perturbation theory we have checked explicitly for finite-size effects and other systematic errors such as sign changes of the fermion determinant. Both were seen to be under control for the scrutinized parameter range. We could confirm earlier weak coupling results and for the first time resolve deviations from perturbation theory. All three kinds of fermions, Wilson, twisted Wilson, and SLAC fermions, approach the same continuum results. It turned out that lattice artifacts were largest for Wilson and smallest for SLAC fermions. At intermediate coupling we observed that the supersymmetrically improved lattice action using Wilson fermions lead to unstable simulations that eventually fail to produce reliable results unless very large lattices are chosen. Simulations with SLAC fermions proved to be much more stable; they allow for improvement terms for a wider parameter range. At finite lattice spacing and weak coupling no significant differences in the measured spectrum between simulations using the improved or unimproved actions could be seen. It is only at larger coupling that deviations become visible, and the improved lattice action in fact suppresses lattice artifacts.

It is still an open problem to go to even stronger couplings. Practical simulations become considerably more involved due to stronger fluctuations in the sign of the fermion determinant. Further refinements of our algorithm are already under investigation, and we hope to report of our progress in the near future. Apart from that, the attainable large statistics allow for the determination of the (constrained) effective potential for this theory; this might serve as an independent check of the non-renormalization theorem for this particular supersym-metric model.

We believe that a generalization of our numerical methods to all supersymmetric theories without gauge fields can be accomplished. In particular, the $\mathcal{N} = 1$ model in both two and four dimensions as well as supersymmetric non-linear sigma models are within reach. At least the experience gained in two-dimensional models suggests that SLAC and twisted Wilson fermions might be good candidates for the formulation of four-dimensional supersymmetric lattice theories.

APPENDIX A: DETERMINATION OF MASSES FROM TWO-POINT CORRELATORS

One important observable of a quantum field theory is the energy gap between the ground state and the first excited state. This energy gap corresponds to the mass of the lightest particle in the spectrum.

To obtain the masses in the Wess-Zumino model one has to consider the propagators of fermions and bosons. At vanishing spatial momentum $p_1 = 0$, the free bosonic continuum propagator in momentum space reads

$$G^\text{boson}(p) = \frac{1}{m^2 + p_0^2} . \quad (A1)$$

The real and imaginary parts φ_1 and φ_2 of φ decouple (the propagator is diagonal and even equal for φ_1, φ_2). The Fourier transform of $G^\text{boson}(p)$ shows the well known exponential decay

$$C^\text{boson}(t) \propto \exp(-m\,|t|) , \quad (A2)$$

where m is the above mentioned mass of the lightest particle. (The space coordinates corresponding to p_1 and p_0 are called x and t, respectively.) In the interacting case this quantity can be obtained on the lattice by measuring the two-point function. The projection onto $p_1 = 0$ can be achieved by averaging over the spatial lattice sites,

$$C_{\alpha\beta}^\text{boson}(t) = \frac{1}{N_\text{s}} \sum_x \langle \varphi_\alpha(0,0)\varphi_\beta(t,x) \rangle , \quad (A3)$$

with α, β labeling components of the bosonic field.

The free fermionic continuum correlator for $p_1 = 0$ is

$$\langle \psi_\alpha \bar\psi_\beta \rangle = G_{\alpha\beta}^\text{fermion}(p_0) = \frac{m - i\gamma_{\alpha\beta}^0 p_0}{m^2 + p_0^2}. \quad (A4)$$

Using the representation of the γ matrices as described after (4) one can read off a direct connection with the bosonic correlator using

$$G^{\text{fermion}}(p_0) := G^{\text{fermion}}_{11}(p_0) + G^{\text{fermion}}_{22}(p_0) = \frac{2m}{m^2 + p_0^2}. \tag{A5}$$

As in the bosonic case on the lattice a summation over the spatial lattice sites yields the projection onto $p_1 = 0$. $C^{\text{fermion}}(t)$ defines the Fourier transform of this object.

1. Fermion masses

The fermionic propagator $C(x)$ is given by

$$\left\langle \psi_\alpha \bar{\psi}_\beta \right\rangle = \left\langle M^{-1}_{\alpha\beta}(\varphi_1, \varphi_2) \right\rangle , \tag{A6}$$

where M is the fermion matrix. The calculation of this quantity requires a high numerical effort for the inversion of large matrices. Fortunately in the weak-coupling limit the fermion matrix is approximately the same as that of the free theory and the statistical fluctuations are rather small. Therefore the necessary statistics to read off a reasonable fermionic correlator is much smaller than for bosons.

After the fermionic correlator in position space is computed the masses can be determined from its long range behavior. Inspired by the continuum connection between fermionic and bosonic correlators, (A5), and the behavior at large distances, (A2), one can consider

$$m_{\text{eff}} = \ln\left(\frac{C^{\text{fermion}}(t)}{C^{\text{fermion}}(t+1)} \right) \tag{A7}$$

with t in a region between zero and $N_t/2$. The mass can then be determined from the average of m_{eff}.

A more elaborate way is a least square fit of the fermionic correlator $C^{\text{fermion}}(t)$ with the function

$$f_{a,m_f}(t) = a \cdot \cosh(m_f(t - N_t/2)) \tag{A8}$$

One better not take the full range of t into account for this fit because it is valid only for large distances (for periodic boundary conditions, from both boundaries of the lattice). One should therefore constrain t to be in $\{1 + t_{\text{skip}}, \ldots, N_t - 1 - t_{\text{skip}}\}$. The choice of t_{skip} is determined by the fringe of the plateau in a plot of the fitting result vs. t_{skip}.

The differences of the different methods to determine the masses are illustrated in Fig. 17. One clearly observes that the effective masses determined according to (A7) do not show a plateau from which the mass can be read off. By contrast, the masses obtained from a cosh fit clearly show this behavior at large t_{skip}. As mentioned above, the effective mass of the bosonic correlator is subject to much larger statistical errors.

2. Boson masses

In order to calculate the bosonic correlators for the determination of the masses the connected two-point function is considered. At large distances, where the masses can be extracted,
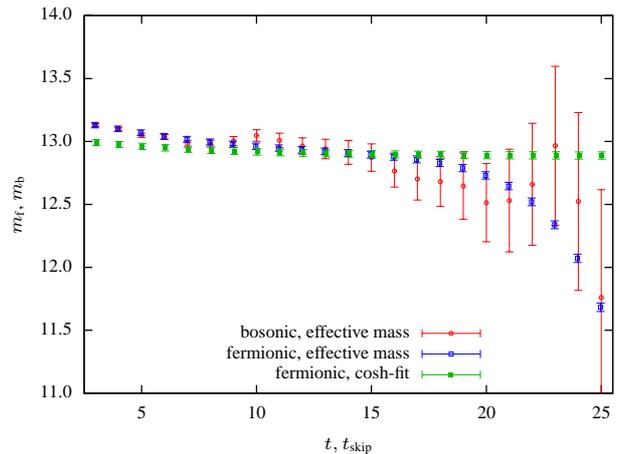
FIG. 17: Bosonic and fermionic masses obtained via a cosh-fit (A8) and the effective mass definition (A7) for the improved Wilson model with $\lambda = 0.4$ on a 64×64 lattice. The fermionic masses with a statistics of about 5,000 independent configurations are much sharper and more reliable than the bosonic effective masses obtained from about 10^6 independent configurations.

the relative statistical error of the correlator grows exponentially. Therefore, one must achieve a balance between this statistical error and the systematical errors due to the evaluation at small distances.

We have fitted $\ln(C^{\text{boson}}(t))$ against the function $A + \ln(\cosh(m_b/N_s(t - N_t/2)))$ to determine A and the effective mass m_b. In order to exclude the points with the largest statistical and systematical errors from this fit, we have taken only the points in the interval $([t_{\text{skip}}, t_{\text{st}}] \cup [N_t - t_{\text{st}}, N_t - t_{\text{skip}}])$ into account. t_{skip} is determined as in the fermionic case and t_{st} such that the statistical error becomes comparably small.

If the SLAC derivative is used an oscillatory behavior of m_b as a function of t_{skip} can be observed. In the bosonic case it is slightly smaller than the statistical error. Therefore, it is sufficient to measure a "smeared" mass, $m_{\text{SLAC}} = 0.5m_b(t_{\text{skip}}, t_{\text{st}}) + 0.25m_b(t_{\text{skip}}+1, t_{\text{st}}) + 0.25m_b(t_{\text{skip}}-1, t_{\text{st}})$, where the error of the oscillations is negligible as compared to the statistical one.

APPENDIX B: CONTINUUM EXTRAPOLATION

For the continuum extrapolation we focus on the fermionic masses because of their much smaller statistical error. The explicit extrapolation procedure is guided by analytic results and observations for the free theory. The three different discretizations investigated in this work require different strategies for this procedure.

1. Wilson derivative

Compared with the continuum formula, (A5), the free momentum space correlation function for the Wilson derivative

gets a momentum dependent mass,

$$G^{\text{fermion}}(p_0) = \frac{m_{\text{latt}} + 1 - \cos(p_0)}{\sin^2(p_0) + (m_{\text{latt}} + 1 - \cos(p_0))^2}. \quad \text{(B1)}$$

The pole of this correlator coincides with the above mentioned cosh-fit within the error bars.

To extrapolate the continuum limit an expansion in powers of the lattice spacing is used. Exact results for the free theory were derived to check this extrapolation. In this case an expansion up to a linear order in a is not enough to obtain the known result within the high precision of the numerical measurements at weak coupling. Therefore we first tried to extended the expansion to a quadratic order which yields a better result; but still the error is to large for our purposes.

The functional behavior of the masses, m_{f}, obtained by the fit as a function of the lattice spacing is well approximated by

$$m_f(a) \approx m_{\text{cont}} + A \cdot a + B \cdot a^{\frac{3}{2}} \quad \text{(B2)}$$

for all $a \in [0, 0.05]$. The deviation from this behavior is negligible with respect to the statistical errors in the weak coupling case. In addition the expected continuum result is achieved with the necessary precision. Motivated by these results this formula is also used in the interacting case.

2. Twisted Wilson derivative

A Wilson parameter of $r = \sqrt{\frac{4}{3}}$ for the twisted Wilson fermions in the free theory leads to discretization errors of $\mathcal{O}(a^4)$ as discussed in [13]. For the weakly coupled regime ($\lambda \le 0.3$) we expect these errors to dominate the lattice artifacts. Nevertheless for an intermediate coupling corrections of $\mathcal{O}(a)$ arise. Taking this into account we extrapolate the masses to continuum assuming a functional behavior of

$$m_f(a) = m_{\text{cont}} + A \cdot a + B \cdot a^4. \quad \text{(B3)}$$

For $\lambda > 0.3$ the $\mathcal{O}(a)$ terms dominate. Therefore a linear extrapolation is sufficient.

3. SLAC derivative

As we have seen in our previous investigations, [13], the SLAC-derivative shows an almost perfect behavior. That means the extrapolated masses coincide with their continuum counterparts already at finite lattice spacings. On the other hand we have observed an oscillatory behavior of the correlation function. This was shown to be connected with the exact reproduction of the continuum dispersion relation by the SLAC derivative. To handle this problem we have again studied the free theory first. As in the bosonic case the plot of m_{f} versus t_{skip} does not show a clear plateau but rather oscillates around the expected continuum value, cf. Fig. 18.

Guided by these observation of the free theory a suitable averaging can lead to the extraction of the correct continuum results at finite lattice spacing. Starting with the ansatz

$$m(N_{\text{s}}, \boldsymbol{c}) := c_0 m_{\text{f}}(t_{\text{skip}}) + c_1 m_{\text{f}}(t_{\text{skip}} - 1) + c_2 m_{\text{f}}(t_{\text{skip}} - 2). \quad \text{(B4)}$$

we minimize the difference form the known continuum result of the free theory

$$\Delta(N_{\text{s}}, \boldsymbol{c}) = |m(N_{\text{s}}, \boldsymbol{c}) - m_{\text{cont}}| \quad \text{(B5)}$$

for lattice sizes of $N_{\text{s}} = N_{\text{t}} \in \{35, 37, \ldots, 75\}$ and $t_{\text{skip}} = \lfloor 0.4 N_{\text{s}} \rfloor$. A least square fit yields

$$c_0 = 0.11791, \quad c_1 = 0.47877, \quad c_2 = 0.40332, \quad \text{(B6)}$$

leading to $\max \Delta(N_{\text{s}}, \boldsymbol{c}) = 5.282 \times 10^{-4}$. A smaller t_{skip} does not change this result considerably. Using this approximation scheme the systematic error based on the oscillatory behavior of the SLAC derivative can be neglected compared to the statistical errors at least for the weak coupling case.
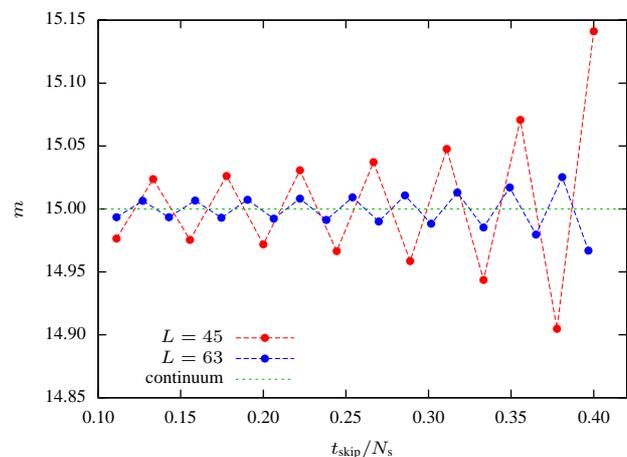
FIG. 18: Masses obtained via a cosh-fit for the free theory using the SLAC derivative. At larger lattices the oscillation amplitude around the continuum value gets smaller.

[1] A. Feo, *Predictions and recent results in SUSY on the lattice*, Mod. Phys. Lett. **A19** (2004) 2387 [arXiv:hep-lat/0410012].

[2] J. Giedt, *Deconstruction and other approaches to supersymmetric lattice field theories*, Int. J. Mod. Phys. **A21** (2006) 3039 [arXiv:hep-lat/0602007].

[3] P. H. Dondi and H. Nicolai, *Lattice supersymmetry*, Nuovo Cim. **A41** (1977) 1.

[4] J. Giedt and E. Poppitz, *Lattice supersymmetry, superfields and renormalization*, JHEP **09** (2004) 029 [arXiv:hep-th/0407135].

[5] I. Montvay, *Tuning to N=2 supersymmetry in the SU(2) ad-*

joint Higgs-Yukawa model, Nucl. Phys. **B445** (1995) 399 [`arXiv:hep-lat/9503009`].

[6] M. F. L. Golterman and D. N. Petcher, *A local interactive lattice model with supersymmetry*, Nucl. Phys. **B319** (1989) 307.

[7] W. Bietenholz, *Exact supersymmetry on the lattice*, Mod. Phys. Lett. **A14** (1999) 51 [`arXiv:hep-lat/9807010`].

[8] G. Bergner, F. Bruckmann and J. M. Pawlowski, *Generalising the Ginsparg-Wilson relation: Lattice supersymmetry from blocking transformations*, `arXiv:0807.1110`.

[9] S. Elitzur, E. Rabinovici and A. Schwimmer, *Supersymmetric models on the lattice*, Phys. Lett. **B119** (1982) 165.

[10] D. B. Kaplan, E. Katz and M. Unsal, *Supersymmetry on a spatial lattice*, JHEP **05** (2003) 037 [`arXiv:hep-lat/0206019`].

[11] H. Nicolai, *On a new characterization of scalar supersymmetric theories*, Phys. Lett. **B89** (1980) 341.

[12] S. Catterall and S. Karamov, *Exact lattice supersymmetry: the two-dimensional N=2 Wess-Zumino model*, Phys. Rev. **D65** (2002) 094501 [`arXiv:hep-lat/0108024`].

[13] G. Bergner, T. Kaestner, S. Uhlmann and A. Wipf, *Low-dimensional supersymmetric lattice models*, Annals Phys. **323** (2008) 946 [`arXiv:0705.2212`].

[14] M. Beccaria, G. Curci and E. D'Ambrosio, *Simulation of supersymmetric models with a local Nicolai map*, Phys. Rev. **D58** (1998) 065009 [`arXiv:hep-lat/9804010`].

[15] S. Duane, A. D. Kennedy, B. J. Pendleton and D. Roweth, *Hybrid Monte Carlo*, Phys. Lett. **B195** (1987) 216.

[16] I. P. Omelyan, I. M. Mryglod and R. Folk, *Symplectic analytically integrable decomposition algorithms: classification, derivation, and application to molecular dynamics, quantum and celestial mechanics simulations*, Computer Physics Communications **151** (2003) 272.

[17] D. H. Weingarten and D. N. Petcher, *Monte Carlo integration for lattice gauge theories with fermions*, Phys. Lett. **B99** (1981) 333.

[18] A. Kirchberg, J. D. Lange and A. Wipf, *From the Dirac operator to Wess-Zumino models on spatial lattices*, Ann. Phys. **316** (2005) 357 [`arXiv:hep-th/0407207`].

[19] S. D. Drell, M. Weinstein and S. Yankielowicz, *Strong coupling field theories. 2. Fermions and gauge fields on a lattice*, Phys. Rev. **D14** (1976) 1627.

[20] J. Giedt, *R-symmetry in the Q-exact (2,2) 2d lattice Wess-Zumino model*, Nucl. Phys. **B726** (2005) 210 [`arXiv:hep-lat/0507016`].

[21] S. Catterall and S. Karamov, *Testing a Fourier accelerated hybrid monte carlo algorithm*, Phys. Lett. **B528** (2002) 301 [`arXiv:hep-lat/0112025`].

[22] S. Cecotti and L. Girardello, *Functional measure, topology and dynamical supersymmetry breaking*, Phys. Lett. **B110** (1982) 39.